Published in final edited form as:
Cell. 2018 September 6; 174(6): 1586–1598.e12. doi:10.1016/j.cell.2018.07.009.

Generation of tumor-reactive T cells by co-culture of peripheral blood lymphocytes and tumor organoids

Krijn K. Dijkstra[#1], **Chiara M. Cattaneo**[#1], **Fleur Weeber**[1], **Myriam Chalabi**[1,2], **Joris van de Haar**[1], **Lorenzo F. Fanchi**[1], **Maarten Slagter**[1], **Daphne L. van der Velden**[1], **Sovann Kaing**[1], **Sander Kelderman**[1], **Nienke van Rooij**[1], **Monique E. van Leerdam**[2], **Annekatrien Depla**[3], **Egbert F. Smit**[4], **Koen J. Hartemink**[5], **Rosa de Groot**[6], **Monika C. Wolkers**[6,7], **Norman Sachs**[8,9], **Petur Snaebjornsson**[10], **Kim Monkhorst**[10], **John Haanen**[1], **Hans Clevers**[8,11,12], **Ton N. Schumacher**[#1,12], and **Emile E. Voest**[#*,1,15]

[1]Department of Molecular Oncology and Immunology, The Netherlands Cancer Institute - Antoni van Leeuwenhoek Hospital, 1066 CX Amsterdam, The Netherlands [2]Department of Gastroenterologic Oncology, The Netherlands Cancer Institute - Antoni van Leeuwenhoek Hospital, 1066 CX Amsterdam, The Netherlands [3]Department of Gastroenterology and Hepatology, 1066 EC Slotervaart Hospital, Amsterdam, The Netherlands [4]Department of Thoracic Oncology, The Netherlands Cancer Institute - Antoni van Leeuwenhoek Hospital, 1066 CX Amsterdam, The Netherlands [5]Department of Surgery, The Netherlands Cancer Institute – Antoni van Leeuwenhoek Hospital, 1066 CX Amsterdam, The Netherlands [6]Department of Hematopoeisis, Sanquin Research, 1066 CX Amsterdam, The Netherlands [7]Landsteiner Laboratory, Amsterdam Medical Center, 1105 AZ Amsterdam, The Netherlands [8]Hubrecht Institute, University Medical Center Utrecht, 3584 CT Utrecht, The Netherlands [10]Department of Pathology, The Netherlands Cancer Institute - Antoni van Leeuwenhoek Hospital, 1066 CX Amsterdam, The Netherlands [11]Princess Maxima Center for Pediatric Oncology, 3584 CS Utrecht, The Netherlands [12]Oncode Institute

[#] These authors contributed equally to this work.

Summary

Cancer immunotherapies have shown substantial clinical activity for a subset of patients with epithelial cancers. Still, technological platforms to study cancer – T cell interactions for individual

[*]Correspondence: e.voest@nki.nl (E.V.).
[9]Present address: Vertex Pharmaceuticals Inc., San Diego, CA 92121, USA
[15]Corresponding author, lead contact

Author contributions

K.D. designed, performed and analysed experiments and wrote the manuscript. C.C. designed, performed and analysed experiments. F.W. designed the clinical protocol and F.W., M.C., D.V., M.L, A.D., E.S., J.H. and K.H. organized patient inclusion. L.F., S.K. and N.R. designed co-culture experiments. J.V.H., L.F. and M.S. analysed DNA sequencing data. S.K. cultured tumor organoids. M.W. and R.G. provided material for and designed reactivity tests against tumor digest. N.S. and H.C. provided protocols for organoid culture. P.S. and K.M. analysed histology data. T.S. and E.V. supervised the study.

Declaration of interests

H.C. is inventor on several patents related to organoid technology.
N.S. reports grants from The Netherlands Organisation for Scientific Research, during the conduct of the study; other from Vertex Pharmaceuticals Incorporated, outside the submitted work; In addition, N.S. has a patent PCT/EP2015/077990 with royalties paid to Stichting HUB, and a patent PCT/EP2015/077988 with royalties paid to Stichting HUB.

Europe PMC Funders Author Manuscripts

patients, and understand determinants of responsiveness, are presently lacking. Here, we establish and validate a platform to induce and analyze tumor-specific T cell responses for epithelial cancers in a personalized manner. We demonstrate that co-cultures of autologous tumor organoids and peripheral blood lymphocytes can be used to enrich for tumor-reactive T cells from peripheral blood of patients with mismatch repair deficient colorectal cancer and non-small cell lung cancer. Furthermore, we demonstrate that these T cells can be used to assess the efficiency of killing of matched tumor organoids. This platform provides an unbiased strategy for the isolation of tumor-reactive T cells and provides a means to assess the sensitivity of tumor cells to T cell-mediated attack at the level of the individual patient.

Introduction

The use of antibodies against immune checkpoints, such as CTLA-4 and PD-1/PD-L1, has shown clear clinical benefit for patients with advanced cancer, including melanoma, non-small cell lung cancer (NSCLC), and mismatch repair deficient (dMMR) colorectal cancer (CRC) (Larkin et al., 2015; Garon et al., 2015; Borghaei et al., 2015; Le et al., 2015; Le et al., 2017; Overman et al., 2017; Overman et al., 2018). Furthermore, adoptive transfer of *ex vivo*-expanded autologous tumor-infiltrating lymphocytes (TIL) has shown impressive clinical responses in melanoma (Rosenberg and Restifo, 2015) and an early clinical signal in cervical cancer (Stevanovic et al., 2015). Despite these encouraging results, a large fraction of patients does not respond to current immunotherapies. Treatment failure may be explained at many different levels that include a low number of immunogenic antigens, defective antigen presentation, and/or the expression of alternative immune checkpoint molecules (Blank et al., 2016; Dijkstra et al., 2016; Pitt et al., 2017; Sharma et al., 2017). Given the large variety in mechanisms of immune evasion by cancers, it is presently challenging to predict whether an individual patient will be sensitive to immunotherapy, what mechanism is likely to underlie resistance and what alternative treatment could potentially overcome such resistance.

Platforms to allow the unbiased and systematic analysis of T cell-mediated tumor recognition on an individual patient basis would greatly contribute to our understanding of the critical factors that determine a successful anti-tumor immune response. Traditionally, *ex vivo* systems to analyze T cell – tumor interaction have to a very large extent focused on cutaneous melanoma, both because of the availability of robust approaches to expand tumor-infiltrating T cells for this disease (Rosenberg and Restifo, 2015), and because of the relative ease with which melanoma cell lines can be obtained. Importantly however, with the now widespread clinical development and clinical use of immunotherapy for major epithelial cancers, it is critical to develop technology to dissect T cell-mediated tumor recognition in these tumor types. Traditionally, this effort has been limited by both the low success rate of establishing primary tumor cell lines of epithelial cancers such as NSCLC and CRC (success rate of 10% or lower) (Dangles-Marie et al., 2007; Zheng et al., 2011), and the limited feasibility of obtaining matched tumor-reactive T cell populations.

We set out to evaluate the feasibility of an autologous T cell – tumor organoid co-culture platform for individual patients. Tumor organoids are three-dimensional primary tumor cell

Europe PMC Funders Author Manuscripts

cultures that retain the histological and mutational features of the original tumor. Organoids can be established from surgical tumor resections (e.g., success rate for CRC of 60-90%) (van de Wetering et al., 2015; Schütte et al., 2017), and from needle biopsies of metastases (e.g. success rate for CRC of ~70%) (Weeber et al., 2015). In this effort, we wished to establish two things: first, whether tumor-reactive T cells can be obtained by co-culture of peripheral blood lymphocytes (PBL) with matched tumor organoids; second, whether such T cells can be used to assess the efficiency of tumor cell killing. The use of peripheral blood as a source of tumor-reactive T cells could provide an easily accessible alternative to TIL. Here we provide proof of concept that co-culture of tumor organoids with PBL forms an unbiased strategy to obtain tumor-reactive T cells from patients with mismatch repair deficient colorectal and non-small cell lung cancer that kill tumor organoids from the same patient. Our findings provide proof of principle for the generation of a novel class of tumor-specific T cell products, derived from peripheral blood, and provide a means to assess the sensitivity of tumor cells to T cell-mediated attack at the level of the individual patient.

Results

Characterization of a panel of mismatch repair deficient (dMMR) CRC organoids

To evaluate whether tumor-reactive T cells can be enriched from PBL by stimulation with autologous tumor organoids, we established a clinical protocol that allowed withdrawing blood and obtaining tumor tissue from patients with CRC. We focused on dMMR CRC given their high mutational load (TCGA, 2012) and frequent response to anti-PD-1 therapy (Le et al., 2015; Le et al., 2017; Overman et al., 2017; Overman et al., 2018). Fresh tumor tissue was obtained from resection specimens or core needle biopsies and used for the establishment of organoids. Mismatch repair deficiency was evaluated by an independent pathologist based on expression of mismatch repair proteins according to standard diagnostic criteria (Table 1 and STAR* Methods). In line with prior data (Weeber et al., 2015; van de Wetering et al., 2015; Schütte et al., 2017), the success rate of growing tumor organoids from these sources was ~60%. Organoids were expanded by weekly to biweekly passaging at 1:2 to 1:5 split ratios and cryopreserved in low passage master biobanks within 2-9 weeks after derivation. Organoids can be recovered from frozen stocks and expanded for several months to large numbers without loss of proliferative capacity.

We established a panel of 15 tumor organoids from 13 different patients with dMMR CRC (Table 1). The organoids morphologically reflected the original tumor they were derived from (Figure 1A and Figure S1). Whole-exome sequencing (WES) of tumor organoids showed a high mutational burden (median 1938 non-synonymous mutations per tumor, range 795-2877), well in the range previously reported for hypermutated CRC (Figure 1B) (TCGA, 2012; Vogelstein et al., 2013). Mutations typically associated with hypermutated CRC (TCGA, 2012) were also represented in these organoids (Figure 1C and Table S1). Considering that loss of MHC-I occurs in up to 60% of dMMR CRC (Dierssen et al., 2007), we screened for MHC-I expression after stimulation with IFNγ and identified 9 MHC-I proficient tumor organoids from 8 patients (62% of organoid samples) (Figure 1D and Figure S2). MHC-I expression of tumor organoids correlated with immunohistochemistry data of MHC-I expression of the tumor they were derived from (Spearman r = 0.78; p =

Europe PMC Funders Author Manuscripts

0.01) (Figure S2 and Table S2). Most importantly, tumor organoids classified as MHC-I-deficient were always derived from MHC-I deficient tumors, indicating that loss of MHC-I is not a general feature of organoid culture.

Induction of tumor reactivity in circulating T cells by co-culture with autologous tumor organoids

To test whether tumor organoids may be used to obtain tumor reactive T cells, we selected MHC-I proficient tumor organoids and focused on the peripheral blood compartment as a source of T cells with a lower degree of exhaustion. Prior to co-culture with autologous T cells, tumor organoids were pre-stimulated with IFNγ to enhance antigen presentation. IFNγ exposure also led to the induction of PD-L1, a negative regulator of T cell activation (Figure 1E), and to counteract any inhibitory effect of PD-L1 during T cell activation, we added blocking antibodies to PD-1. Plate-bound anti-CD28 and IL-2 were added to provide co-stimulation and to support T cell proliferation, respectively. Peripheral blood mononuclear cells (PBMC) were isolated from patients with dMMR CRC and stimulated weekly with autologous tumor organoids (Figure 2A). Tumor recognition by $CD8^+$ T cells was evaluated at baseline and after two weeks of co-culture, by staining for IFNγ and the degranulation marker CD107a.

In four out of eight (50%) patients with MHC-I^+ tumor organoids, stimulation with autologous tumor organoids induced both IFNγ secretion and CD107a upregulation in $CD8^+$ T cells after two weeks of co-culture (Figure 2B-C). Responses were never observed in MHC-I deficient lines (data not shown). The magnitude of the response varied between patients, including small but reproducible responses of 1-3% tumor-reactive $CD8^+$ T cells, as well as a patient of whom ~50% of all $CD8^+$ T cells were tumor-reactive. The high reactivity for CRC-9 suggested the presence of a pre-existing tumor-reactive T cell population. We therefore evaluated tumor reactivity of T cells before co-culture with tumor organoids (i.e. directly after isolation from blood). A substantial proportion of $CD8^+$ T cells from patient CRC-9 was already tumor-reactive, and this population increased approximately 10-fold in frequency upon two weeks of co-culture (Figure 2D-E). In contrast, T cells from patients CRC-11, CRC-12 and CRC-13 did not show any detectable tumor reactivity before organoid co-culture (Figure 2E), indicating that T cell – organoid co-culture systems can also be used to expand previously undetectable tumor-reactive T cell populations.

Induction of tumor reactivity in circulating T cells from patients with NSCLC

We then assessed whether our strategy to obtain tumor-reactive T cell populations from peripheral blood by organoid co-culture could also be applied to non-small cell lung cancer. As compared to dMMR CRC, mutational burden of NSCLC is approximately 5-fold lower (Vogelstein et al., 2013; Govindan et al., 2012) and response to PD-1/PD-L1 blockade is restricted to approximately 20% of patients (Garon et al., 2015; Borghaei et al., 2015). We generated NSCLC organoids from six patients (Figure 3A, Table S3 and Figure S3), using a method similar to that established for CRC organoids (Sachs et al., 2018). Sample NSCLC-3 contained both normal airway epithelial organoids that grew as cystic thin-walled organoids and tumor organoids that showed a more solid morphology. To select for tumor organoids, we applied the MDM-2 inhibitor Nutlin-3a to selectively grow out p53-mutant cells of this

Europe PMC Funders Author Manuscripts

sample, resulting in a pure tumor organoid population (Sachs et al., 2018). All NSCLC organoids were MHC-I proficient and expressed various levels of PD-L1 upon stimulation with IFNγ (Figure 3B-C). In vitro exposure of PBMC to autologous tumor organoids resulted in the expansion of tumor-reactive $CD8^+$ populations in two of these patients after two weeks of co-culture (Figure 3D-E). Notably, none of these responses could be consistently detected before co-culture with organoids (Figure 3F). Collectively, these data demonstrate the feasibility of inducing patient-specific tumor-reactive T cell responses by co-culture of PBMC and autologous tumor organoids in two epithelial tumor types.

Specificity of organoid-reactive T cell responses

We next wished to evaluate whether the T cell responses induced by organoid co-culture are truly tumor-specific or should be considered artefacts of organoid culture or IFNγ treatment. Specifically, while IFNγ enhances antigen processing and presentation, it also induces expression of a large number of genes, potentially allowing the formation of T cell responses against (self) antigens not expressed in the absence of IFNγ. To evaluate the dependency of tumor organoid-reactive T cell responses on IFNγ, we compared T cell expression of the activation marker CD137 upon stimulation with tumor organoids that were either pre-stimulated with IFNγ or left untreated (Figure 4A). For 4 out of 5 cases tested, similar $CD8^+$ T cell responses were induced toward tumor organoids regardless of IFNγ pre-stimulation. To more directly assess whether the induced T cell responses were specific for tumor antigens, we tested whether T cells also responded to stimulation with organoids of autologous normal tissue, and whether T cells responded to stimulation with autologous tumor digest. To assess restriction of T cell reactivity to the tumor organoid used for T cell induction, we established normal colon or lung organoids from two patients (CRC-12 and NSCLC-3). In addition, we generated organoids of a synchronous mismatch repair proficient (pMMR) CRC from patient CRC-13, from whom we also had obtained a dMMR CRC. In all cases, T cell reactivity was restricted to the tumor organoids to which reactivity had been induced in the two-week co-culture with PBL, i.e. no reactivity was observed against normal tissue or pMMR CRC organoids (Figure 4B-G).

For two patients, single cell digest of autologous tumor tissue was also available to stimulate organoid-reactive T cells (Figure 4F-G). T cells reactive to NSCLC-3 organoids were also reactive to tumor digest but not to normal lung digest. In contrast, T cells reactive to NSCLC-1 organoids did not produce IFNγ upon stimulation with autologous tumor digest. While the relatively low level of reactivity towards NSCLC-1 organoids limits the ability to detect subtle reactivity towards tumor digest, at this stage we cannot rule out that T cell reactivity in this sample is directed against organoid-specific targets. Taken together with the experiments in which we evaluated reactivity toward control organoids, this indicates that for 3 out of 4 tested samples, induced $CD8^+$ T cell responses are tumor-specific. At the same time, it also highlights the value of generating organoids from non-malignant tissue that can serve as controls.

$CD4^+$ T cell reactivity against xenogeneic tissue culture components

In addition to tumor-reactive $CD8^+$ T cell responses, we occasionally observed variable $CD4^+$ T cell responses upon stimulation with tumor organoids (Figure 5A). Notably, $CD4^+$

T cell reactivity was not restricted to tumor organoids, but was in some cases also directed against control organoids (organoids of normal tissue or of the synchronous pMMR CRC from patient CRC-13) (Figure 5B). Since we only observed cross-reactivity to control organoids for $CD4^+$ T cells and not for $CD8^+$ T cells, we hypothesized this may be directed against foreign antigens derived from the extracellular environment. Organoids are cultured in murine basement membrane matrix (Geltrex), and consequently murine antigens could be presented to T cells. To address this hypothesis, we generated monocyte-derived dendritic cells (moDCs) from PBMC of patient CRC-1 and loaded these with Geltrex, or irradiated cells of tumor or healthy colon organoids. $CD4^+$ T cell reactivity was only induced by stimulation with Geltrex-loaded DCs or organoids grown in Geltrex (Figure 5C). In addition, reactivity was largely abolished when organoids were grown in the absence of Geltrex for three days (Figure 5C and Figure S4). This indicates that co-culture systems involving Geltrex can induce $CD4^+$ T cell reactivity that is not directed against tumor antigens. Of note, strategies to expand organoids in synthetic matrices have been described recently (Gjorevski et al., 2016) and could serve as alternatives to bypass reactivity to animal antigen.

Tumor organoids are killed by autologous tumor-reactive T cells

Having established the feasibility of inducing autologous tumor-reactive $CD8^+$ T cell products for a substantial fraction of patients, we next aimed to determine whether organoid systems can be used to assess the efficiency of tumor destruction by these T cells. To determine this, we co-cultured tumor organoids with autologous tumor-reactive T cell populations for three days and quantified the number of live tumor cells by flow cytometry. For all samples tested, exposure of tumor organoids to autologous T cells led to substantially reduced survival (Figure 6A). Addition of MHC-I blocking antibodies rescued tumor cell survival, demonstrating the presence of an antigen-specific $CD8^+$ T cell response. To visualize the cytolytic activity of tumor-reactive T cells, NSCLC-1 organoids were labelled with a tracer dye and imaged in the presence of a green-fluorescent apoptosis probe detecting active caspase 3/7 (“caspase 3/7 probe”) (Figure 6B). Addition of autologous T cells led to reduced organoid size and was accompanied by widespread apoptosis.

To provide further evidence for the specificity of tumor cell killing by autologous T cells, we performed parallel cytotoxicity assays with tumor and healthy organoids of NSCLC-3. T cells were first expanded using the rapid expansion protocol previously established to generate TIL products for adoptive cell therapy (Dudley et al., 2003). T cells efficiently killed tumor organoids, but did not affect survival of healthy organoids (Fig. 6C). Live imaging showed strong T-cell mediated killing of tumor organoids when incubated with autologous T cells (Figure 6D, Figure S5 and Video S1). Tumor organoids cultured without T cells (Video S2) or with T cells in the presence of blocking antibodies to MHC-I and MHC-II (Video S3) continued to proliferate. As a further control, healthy organoids continued proliferation regardless of the presence of T cells (Figure 6D, Figure S5 and Videos S4-6). Taken together, these data demonstrate that organoids of epithelial tumors can be used to measure the rate of destruction by autologous T cells. This platform should provide a valuable tool to compare e.g. the relative contribution of different cancer (neo-)antigens to T cell-mediated killing, to assess how the genetic state of tumor cells

influences sensitivity to T cell attack, and to test the value of strategies to increase this sensitivity.

Discussion

The potential of patient-specific model systems for the implementation of personalized medicine in the field of targeted therapy is considered substantial (Horvath et al., 2016). We speculate that the value of patient-specific model systems will prove even higher in the field of immuno-oncology, given the inherent diversity in HLA and TCR genes, the private nature of the neo-antigens that are expressed in human cancers, and the multifactorial nature of T cell-mediated tumor destruction. Much of our current understanding of T cell recognition in human cancer has been based on work in melanoma, and robust systems to measure T cell – tumor interactions in a patient-specific manner have to our knowledge not been described for epithelial cancers. Here we provide proof of concept that tumor organoids can be used to establish individualized *ex vivo* model systems to support T cell-based therapies and to study the interactions between T cells and tumor cells.

We foresee two major applications for the platform that we describe. First, it will allow one to mechanistically dissect the pathways that determine tumor cell sensitivity and resistance to immunotherapy. Second, it opens the possibility to generate patient-specific T cell products in an unbiased manner. With respect to the former application, the ability to establish tumor organoid cultures from very limited amounts of tumor (such as needle biopsies), combined with the potential to expand circulating tumor-reactive T cells from peripheral blood, provides a minimally invasive means to interrogate tumor sensitivity to immunotherapy for individual patients at different time points during treatment. For patients who initially responded to treatment with immune checkpoint inhibitors but eventually relapse, the establishment of co-cultures based on paired (tumor and blood) biopsies before and after relapse should provide a unique assay system for the functional dissection of the underlying cause of relapse. Recent genetic studies on paired biopsies have demonstrated the power of such an approach in a small set of melanoma patients who relapsed while on anti-PD1 therapy, demonstrating the acquisition of JAK1/2 mutations as one cause of resistance (Zaretsky et al., 2016). It will be of interest to determine whether a similar reduced sensitivity to T cell attack by JAK1/2 mutations is selected for in epithelial cancers. In addition to the analysis of natural and therapy-induced variation in tumor cell sensitivity to T cell pressure, there is increasing interest in the use of small molecules and antibodies to enhance tumor cell sensitivity to T cell attack (Patel and Minn, 2018). Parallel tumor organoid – T cell cultures in the presence or absence of drugs of interest should form a straightforward system to identify suitable candidates for combination with immunotherapy.

With respect to the second potential application of this platform, the ability to expand circulating tumor-reactive T cells by co-culture with tumor organoids provides a clinically feasible strategy for the generation of patient-specific T cell products for adoptive T cell transfer. This approach bypasses the need for samples derived from resection specimens to isolate tumor-infiltrating lymphocytes. In our proof of concept study, tumor-reactive $CD8^+$ T cells were expanded from the circulation in four out of thirteen dMMR CRC patients (31%) and two out of six NSCLC patients (33%). When considering only MHC-I proficient dMMR

Europe PMC Funders Author Manuscripts

CRC patients, tumor-reactive T cells were induced in 50% of samples, highlighting the need for strategies to revert or bypass MHC-I loss as an immune escape mechanism. Larger sample sizes will be needed to more precisely define the success rate of this approach. Moreover, in this study we focused on tumor types with high mutational load, and it will be important to determine whether the feasibility of inducing tumor-reactive T cells can be extended to poorly immunogenic cancers, such as mismatch repair proficient colorectal cancer. In parallel, efforts to further increase the success rate of this approach could focus on strategies to improve selection of circulating tumor-reactive T cells, for example based on PD-1 expression by T cells (Gros et al., 2016).

STAR* Methods

Key Resources Table

REAGENT or RESOURCE	SOURCE	IDENTIFIER
Antibodies		
Mouse anti-human MLH1	Roche	M1; Cat#6472966001
Mouse anti-human MSH2	Roche	G219-1129; Cat#5269270001
Mouse anti-human MSH6	Abcam	EP49; Cat#AC-0047
Mouse anti-human PMS2	Agilent Technologies	EP51; Cat# M3647
Mouse anti-human CD28	eBioscience	CD28.2; Cat#16-0289-81
Mouse anti-human HLA-ABC (PE-conjugated)	BD	G46-2.6; Cat#555553
Mouse anti-human CD274 (PD-L1) (APC-conjugated)	eBioscience	MIH1; Cat#17-5983-41
Mouse IgG1 κ isotype control (PE-conjugated)	BD	MOPC-21; Cat#556650
Mouse IgG1 κ isotype control (APC-conjugated)	eBioscience	P3.6.2.8.1; Cat#17-4714-41
Mouse anti-human CD107a (PE-conjugated)	BD	H4A3; Cat#555801
Mouse anti-human CD3 (PerCP-Cy5.5-conjugated)	eBioscience	SK7; Cat#332771
Mouse anti-human CD4 (FITC-conjugated)	BD	RPA-T4; Cat#555346
Mouse anti-human CD8 (BV421-conjugated)	BD	RPA-T8; Cat#562429
Mouse anti-human IFNγ (APC-conjugated)	BD	B27; Cat#554702
Mouse anti-human CD137 (APC-conjugated)	BD	4B4-1; Cat#550890
Mouse anti-human CD3	eBioscience	OKT-3; Cat#16-0037-85
Mouse anti-human HLA-ABC	The Netherlands Cancer Institute	W6/32
Mouse anti-human HLA-DR/DP/DQ (sodium azide free)	BD	Tü39; Cat#555556
Mouse anti-human CD3 (Alexa Fluor 700-conjugated)	Invitrogen	UCHT1; Cat#CD0329
Mouse anti-human CD326 (EpCAM) (PE/Cy7-conjugated)	Biolegend	9C4; Cat#324222

Europe PMC Funders Author Manuscripts

REAGENT or RESOURCE	SOURCE	IDENTIFIER
Anti-human PD1	Merus	N/A
Mouse anti-human HLA-ABC	Nordic Mubio	HCA2; Cat#MUB2036P
Mouse anti-human HLA-ABC	Nordic Mubio	HC10; Cat#MUB2037P
Mouse anti-human p53	Agilent Technologies	DO-7
Biological Samples		
Patient tumor and normal colon or lung tissue	The Netherlands Cancer Institute	study NL48824.031.14
Patient blood	The Netherlands Cancer Institute	study NL48824.031.14
Healthy donor blood (buffy coat)	Sanquin blood bank	N/A
Chemicals, Peptides, and Recombinant Proteins		
B27 supplement without vitamin A	Gibco	Cat#C12587-010
B27 supplement	Gibco	Cat#17504-044
N-Acetylcysteine	Sigma-Aldrich	Cat#A9165-5G
Nicotinamide	Sigma-Aldrich	Cat#N0636
Human recombinant EGF	Peprotech	Cat#AF-100-15
A83-01	Tocris	Cat#2939
SB202190	Cayman Chemicals	Cat#10010399
Prostaglandin E2	Cayman Cehmicals	Cat#14010-1
Y-27632	Sigma-Aldrich	Cat#Y-0503
Human recombinant FGF-7	Peprotech	Cat#100-19
Human recombinant FGF-10	Peprotech	Cat#100-26
Geltrex LDEV-free reduced growth factor basement membrane	Gibco	Cat#A1413202
Collagenase type II	Sigma-Aldrich	Cat#C6885
Hyaluronidase type IV	Sigma-Aldrich	Cat#H3506
Advanced DMEM-F12	Gibco	Cat#12634-028
Penicillin/streptomycin	Gibco	Cat#15070063
Ultraglutamine type I	Lonza	Cat#BE17-605E
HEPES	Gibco	Cat#15630-056
TrypLE Express	Gibco	Cat#12604-013
Recovery Cell Culture Freezing Medium	Gibco	Cat#12648-010
Nutlin-3a	Cayman Chemicals	Cat#10004372
RPMI 1640	Gibco	Cat#11875093
Human serum, from human male AB plasma	Sigma-Aldrich	Cat#H3667
Benzonase	Merck	Cat#70746-3
Human recombinant interferon gamma	Peprotech	Cat#300-02
GolgiSTOP (Monensin)	BD	Cat#554724
GolgiPLUG (Brefeldin A)	BD	Cat#555029

Europe PMC Funders Author Manuscripts

REAGENT or RESOURCE	SOURCE	IDENTIFIER
Phorbol 12-myristate 13-acetate (PMA)	Sigma-Aldrich	Cat#19-144
Ionomycin	Sigma-Aldrich	Cat#I9657
Dispase type II	Sigma-Aldrich	Cat#D4693
Cell Recovery Solution	Corning	Cat#354253
GMP DC medium	CellGenix	Cat#20801-0500
Recombinant human GM-CSF	CellGenix	Cat#1012-050
Recombinant human IL-1β	CellGenix	Cat#1011-050
Recombinant human IL-4	CellGenix	Cat#1003-050
Recombinant human TNF-α	CellGenix	Cat#1006-050
Recombinant human IL-6	CellGenix	Cat#1004-060
Interleukin-2		Proleukin
Prostaglandin E1		Alprostadil
Critical Commercial Assays		
DNeasy blood and tissue kit	Qiagen	Cat#69504
Fixation/Permeabilization solution kit	BD	Cat#554714
Live/dead fixable near-IR dead cell stain kit	Invitrogen	Cat#L10119
CD137 Microbead kit, human	Miltenyi	Cat#130-093-476
CellTrace Yellow Cell Proliferation Kit	Invitrogen	Cat#C34567
CellTrace Far Red Cell Proliferation Kit	Invitrogen	Cat#C34564
AccuCount blank particles (7.0 – 7.9 μm)	Spherotech	Cat#ACBP-70-10
NucView488 Caspase-3 assay kit	Biotium	Cat#30029
Experimental Models: Cell Lines		
L-Wnt3a cell line	Laboratory of Hans Clevers, Hubrecht Institute	L-Wnt3a
R-spondin producer cell line	Laboratory of Calvin Kuo, Stanford	293T-HA-RspoI-Fc
Noggin producer cell line	Laboratory of Hans Clevers, Hubrecht Institute	HEK293-mNoggin-Fc
Software and Algorithms		
Optitype	Szolek et al. 2014	https://github.com/F RED-2/OptiType
Somatic Sniper	Larson et al. 2012	http://gmt.genome.wustl.edu/packages/somatic-sniper/
Somatic Indel Detector (GATK)	McKenna et al. 2010	https://software.broadinstitute.org/gatk/
snpEff, version 4.3	Cingolani et al. 2012	http://snpeff.sourceforge.net
FlowJo version 10		https://www.flowjo.com/
ImageJ version 1.50i	Schneider et al. 2012	https://imagej.nih.gov/ij/

Contact for reagent and resource sharing

Further information and requests for resources and reagents should be directed to and will be fulfilled by the Lead Contact, Emile E. Voest (e.voest@nki.nl).

Reagents obtained under material transfer agreement (MTA) include producer lines for conditioned medium of Wnt-3a, Noggin (MTA with Hubrecht Institute) and R-spondin-1 (MTA with Calvin Kuo, Stanford).

Patient material, including tissue and organoids, are available for sharing as defined in the signed informed consent (study NL48824.031.14), and as approved by the local Medical Ethical Committee. Deposition of DNA sequencing data in publicly available databases is regulated by the informed consent that participants to this study signed.

Experimental model and subject details

Human subjects—The study (NL48824.031.14) was approved by the Medical Ethical Committee of The Netherlands Cancer Institute – Antoni van Leeuwenhoek hospital and written informed consent was obtained from all patients. Peripheral blood and tumor tissue were obtained from patients with a confirmed diagnosis of colorectal or non-small cell lung cancer. Mismatch repair deficiency was confirmed by immunohistochemical staining for the mismatch repair proteins MSH2, MSH6, MLH1 and PMS2 in routine assessment by a pathologist (see Immunohistochemistry).

Organoid culture—Tumor tissue was obtained either by 18G core needle biopsy or by surgical resection. Tumor tissue was processed for organoid culture within 24 hours. CRC organoids were established essentially as described in van de Wetering et al. 2015. NSCLC organoids were cultured using similar methods; a detailed protocol is accessible at bioRxiv (Sachs et al., 2018). Briefly, tumor tissue derived from needle biopsies was mechanically dissociated into small tumor pieces using needles and embedded in Geltrex (Geltrex LDEV-free reduced growth factor basement membrane extract, Gibco). Tumor tissue derived from surgical resections was cut into small pieces and enzymatically digested using 1.5 mg/mL collagenase II (Sigma-Aldrich), 10 μg/mL hyaluronidase type IV (Sigma-Aldrich) and 10 μM Y-27632 (Sigma-Aldrich) before embedding in Geltrex. After Geltrex solidification for 20 minutes at 37 °C, cells were overlaid with human colorectal cancer (CRC) or non-small cell lung cancer (NSCLC) organoid medium (van de Wetering et al., 2015; Sachs et al., 2018). Human CRC organoids medium is composed of Ad-DF+++ (Advanced DMEM/F12 (Gibco) supplemented with 2 mM Ultraglutamine I (Lonza), 10 mM HEPES (Gibco), and 100/100 U/ml Pencillin/Streptomycin (Gibco)), 10% Noggin-conditioned medium, 20% R-spondin1-conditioned medium, 1x B27 supplement without vitamin A (Gibco), 1.25 mM N-Acetylcysteine (Sigma-Aldrich), 10 mM nicotinamide (Sigma-Aldrich), 50 ng/mL human recombinant EGF (Peprotech), 500 nM A83-01 (Tocris), 3 μM SB202190 (Cayman Chemicals) and 10 nM prostaglandin E2 (Cayman Chemicals). Human wild-type colon organoid medium is identical to CRC medium, except that 50% Wnt3a-conditioned medium is added. Human NSCLC and normal airway organoid medium is composed of Ad-DF+++, 10% Noggin-conditioned medium, 10% R-spondin1-conditioned medium, 1x B27 supplement, 1.25 mM N-Acetylcystein, 10 mM nicotinamide, 25 ng/mL human recombinant

FGF-7 (Peprotech), 100 ng/mL human recombinant FGF-10 (Peprotech), 500 nM A83-01, 1 μM SB202190, 5 μM Y-27632. R-spondin1-conditioned medium was produced from 293T-HA-RspoI-Fc producer cell lines (obtained from C. Kuo, Stanford), Wnt3a-conditioned medium from L-Wnt3a cells and Noggin-conditioned medium from HEK293-mNoggin-Fc cell lines (both kind gift from J. den Hertog, Utrecht). In the first two weeks of organoid culture, 1x Primocin (Invivogen) was added to prevent microbial contamination. Organoids were passaged approximately every week by incubating in TrypLE Express (Gibco) for 5-10 minutes at 37 °C to dissociate organoids to single cells and replating in fresh Geltrex. After passaging, 10 μM Y-27632 was added to CRC medium for the first 2-3 days. Organoids were cryopreserved in 10%FCS/DMSO or Recovery Cell Culture Freezing Medium (ThermoFisher) as master and working biobanks. Organoids < passage 30 were used in experiments. To rule out overgrowth by healthy lung organoids for NSCLC organoids derived from intrapulmonal lesions, haematoxylin and eosin stained sections of tumor organoids (see Immunohistochemistry) were evaluated by a pathologist to determine tumor status of organoids. To prevent overgrowth by healthy lung organoids, for patient NSCLC-3, p53-mutant organoids were selected by culturing in the presence of 5 μM Nutlin-3 (Cayman Chemicals). Organoids were regularly checked for mycoplasma contamination using the MycoAlert Mycoplasma Detection Kit (Lonza).

Peripheral blood lymphocytes—The peripheral blood mononuclear cells (PBMC) fraction was isolated from peripheral blood by Ficoll-Paque density gradient separation and cryopreserved until later use.

Organoid line authentication—DNA was isolated from master and working biobanks of organoids and patient-matched peripheral blood using a DNEasy kit (Qiagen). Samples were genotyped using a Taqman-based SNParray targeting 26 SNPs (Hartwig Medical Foundation, Amsterdam). An identity score was calculated as described by (Tanabe et al., 1999) and (Liang-Chu et al., 2015). When comparing two samples, for each locus where both samples had called alleles, the number of distinct alleles in each individual sample, as well as the number of shared alleles was computed. These were summed across all loci and an identity score was computed defined as

$$\frac{2x\ the\ number\ of\ shared\ alleles}{total\ distinct\ alleles\ sample\ 1 + total\ distinct\ alleles\ sample\ 2}$$

A threshold of 0.9 of the summed identity score was defined as a cut-off and organoid lines that did not match to autologous blood were discarded.

Two samples (NSCLC-3 and NSCLC-5), showed identity scores < 0.9 in comparison with autologous blood, but showed exclusively heterozygous to homozygous changes in the tumor, suggesting loss of heterozygosity due to copy number aberrations. We authenticated these lines by performing HLA-typing by PCR (Sanquin, Amsterdam) or based on whole genome sequencing data by Optitype (Szolek et al. 2014).

Europe PMC Funders Author Manuscripts

Method details

Organoid – lymphocyte co-culture—Culture media for PBMC was composed of RPMI 1640 (Gibco), supplemented with 2 mM Ultraglutamine I, 1:100 penicillin/streptomycin and 10% male human AB serum (Sigma-Aldrich) ("T cell medium"). One day before co-culture, PBMC were thawed in pre-warmed (37 °C) T cell medium (human serum was replaced with FCS during thawing) and incubated for 15 minutes with 25 U/mL benzonase (Merck). After washing, cells were resuspended at 2-3*10^6 cells/mL in T cell medium supplemented with 150 U/mL IL-2 and cultured overnight at 37 °C. Prior to co-culture, tumor organoids were stimulated overnight with 200 ng/mL human recombinant IFNγ (Peprotech). 96-well U-bottom plates were coated with 5 μg/mL anti-CD28 (clone CD28.2, eBioscience) and kept overnight at 4 °C.

The next day, tumor organoids were dissociated to single cells with TrypLE Express and resuspended in T cell medium. Anti-CD28-coated plates were washed twice with PBS and PBMC were seeded at a density of 10^5 cells/well and stimulated with single cell-dissociated organoids at a 20:1 effector:target ratio. Co-cultures were performed in the presence of 150 U/mL IL-2 and 20 μg/mL anti-PD-1-blocking antibody (kindly donated by Merus, Utrecht). Half of the medium, including IL-2 and anti-PD-1, was refreshed two to three times per week. Every week, PBMC were collected, counted and replated at 10^5 cells/well, and re-stimulated with fresh tumor organoids.

Flow cytometry—For evaluation of MHC-I and PD-L1 expression by tumor organoids, organoids were dissociated to single cells using TrypLE Express, with or without overnight pre-incubation with 200 ng/mL IFNγ. Tumor cells were washed in FACS buffer (PBS + 5 mM EDTA + 1% bovine serum antigen) and stained with mouse anti-human HLA-A,B,C-PE (BD Bioscience) or anti-CD274-APC (eBioscience) antibodies, or isotype controls (PE mouse IgG1, kappa (BD) and APC mouse IgG1 kappa (eBioscience)) for 30 minutes at 4 °C. Cells were washed twice with FACS buffer and DAPI was added to exclude dead cells prior to recording at a Becton Dickinson Fortessa or LSRII flow cytometer.

For evaluation of tumor reactivity, 10^5 PBMC were restimulated with tumor organoids at a 2:1 effector: target ratio and seeded in anti-CD28-coated plates in the presence of 20 μg/mL anti-PD-1 and co-cultured for 5 hours. Mouse anti-human CD107a-PE antibodies (BD) were added at the start of co-culture. Golgi-Plug (1:1000, BD) and Golgi-Stop (1:1500, BD) was added after 1 hour and co-culture continued for an additional 4 hours. Cells were washed twice in FACS buffer and stained with the following antibodies: anti-CD3-PerCP-Cy5.5 (BD), anti-CD4-FITC (BD), anti-CD8-BV421 (BD), and near-IR viability dye (Life technologies) for 30 minutes at 4 °C. Cells were washed twice in FACS buffer, fixed and stained for intracellular IFNγ (anti-IFNγ-APC, BD) using the Cytofix/Cytoperm kit (BD), according to manufacturer's instructions. PBMC stimulated with 50 ng/mL phorbol 12-myristate 13-acetate (PMA, Sigma-Aldrich) and 1 μg/mL ionomycin (Sigma-Aldrich) served as positive controls and PBMC cultured without tumor stimulation as negative controls. In some experiments, PBMC and tumor cells were co-cultured for 24 hours before staining with anti-CD3-PerCP-Cy5.5, anti-CD4-FITC, anti-CD8-PB, anti-CD137-APC (BD) and near-IR viability dye.

Rapid expansion of unselected T cells or tumor-reactive sublines—T cells from patient CRC-12, NSCLC-1 and NSCLC-3 were co-cultured for two weeks with autologous tumor organoids and expanded for two weeks in the presence of irradiated (40 Gy, Gamma Cell-40) pooled PBMC from three healthy donors (1:200 T cell:feeder ratio), 3000 U/mL IL-2 and 30 ng/mL anti-human CD3 (OKT-3, eBioscience). After 5-7 days, medium, including IL-2, was refreshed every 2-3 days. For expansion of tumor-reactive sublines, T cells were sorted on the basis of CD137 expression 24 hours after stimulation with tumor organoids, using a CD137 Microbead Kit (Miltenyi) following manufacturer's instructions and expanded as described above.

Organoid killing assays—To determine the sensitivity of tumor organoids to T cell-mediated killing, flat-bottom non-tissue culture-treated plates were coated with 5 μg/mL anti-CD28 and kept at 4 °C overnight prior to co-culture. Organoids were stimulated with 200 ng/mL IFNγ for 24h prior to co-culture. The next day, organoids were isolated from Geltrex by density gradient separation. Part of the organoids were dissociated to single cells and counted using a hemocytometer. This was used to infer the number of tumor cells per tumor organoid to allow co-culture of organoids and T cells at a 5:1 effector:target ratio. Next, tumor organoids were resuspended in T cell medium. T cells were collected after two weeks of co-culture with tumor organoids and resuspended in T cell medium. Anti-CD28-coated plates were washed twice with PBS and organoids were seeded in triplicate without T cells or with $5*10^4$ autologous T cells obtained by two weeks of organoid co-culture. To block MHC class I and II, organoids were pre-incubated for 30 minutes with 50 μg/mL pan-MHC-I blocking antibody W6/32, or pan-MHC-II blocking antibody Tü39 (blocking antibody remained present throughout the co-culture). To facilitate visualization, organoids were in some cases stained with 1 μM of CellTrace Yellow (Invitrogen) and T cells with 100 nM CellTrace FarRed (Invitrogen) in PBS for 20 minutes at 37 °C followed by blocking with human serum and washing in PBS. At the start of co-culture, a green-fluorescent caspase 3/7 probe that binds DNA upon cleavage by caspase 3/7 (referred to as "caspase 3/7 probe") (Biotium) was added at 1:2000 dilution to visualize cells undergoing apoptosis.

After 3 days of co-culture, organoids and PBMC were collected and dissociated into single cells with TrypLE Express, combined with regular resuspension and vortexing. Care was taken to limit the reaction until the moment organoids were fully dissociated. 7.46 μm AccuCount blank counting beads (Spherotech) were added to each well, cells were washed in FACS buffer and stained with anti-CD3-AF700 (Invitrogen) and anti-CD326-PE-Cy7 (Biolegend) for 30 minutes at 4 °C. Organoids or T cells labelled with CellTrace dyes were not stained with antibodies. Cells were washed twice and stained with DAPI to mark dead cells prior to flow cytometric recording.

Immunohistochemistry—Organoids were recovered from Geltrex by density gradient separation (centrifugation at 300g, 5 minutes, 4 °C in cold basal organoid culture medium) when they reached an approximate diameter of 100 μm, fixed in 4% paraformaldehyde for 30 minutes at room temperature or overnight at 4 °C, pelleted, and embedded in paraffin blocks. In some cases, organoids were isolated from Geltrex using 10 mg/mL dispase type II (Sigma) or Cell Recovery Solution (Corning). Immunohistochemistry of samples was

performed on a BenchMark Ultra autostainer (Ventana Medical Systems). Briefly, paraffin sections were cut at 3 μm, heated at 75°C for 28 minutes and deparaffinized in the instrument with EZ prep solution (Ventana Medical Systems). Heat-induced antigen retrieval was carried out using Cell Conditioning 1 (CC1, Ventana Medical Systems) for 32 minutes at 95°C. P53 was detected using clone DO-7 (1:7000 dilution, 32 minutes at 37°C, Agilent Technologies), and MHC-I using clone HCA2 (1:5000 dilution, 32 minutes at 37°C, Nordic Mubio) and clone HC10 (1:20000 dilution, 32 minutes at 37°C, Nordic Mubio). For HCA2 signal amplification was applied using the Optiview Amplification Kit (4 minutes, Ventana Medical Systems). Bound antibody was detected using the OptiView DAB Detection Kit (Ventana Medical Systems). Slides were counterstained with Hematoxylin and Bluing Reagent (Ventana Medical Systems). For assessment of mismatch repair status, immunohistochemistry was performed according to standard protocols for the Ventana automated immunostainer. (MLH1, clone M1, Roche; MSH2, clone G219-1129, Roche; MSH6, clone EP49, Abcam; PMS2, clone EP51, Agilent Technologies).

Whole exome DNA sequencing—At least 200 ng of genomic DNA was extracted from CRC organoids and patient-matched PBMC using a DNEasy kit (Qiagen). After exome capture (Integrated DNA Technologies probe set), whole-exome sequencing was performed on an Illumina HiSeq DNA analyzer using 100 bp paired-end reads.

T cell recognition assays of Geltrex—Tumor or healthy organoids were isolated from Geltrex using 10 mg/mL dispase type II (Sigma) and cultured in organoid medium for three days with 10 μM Y-27632 (Cayman Chemicals) in 6-well plates. In some cases, two days later, 100 μL/well Geltrex was added to organoids. After three days, organoids were used in tumor recognition assays as described under flow cytometry.

Monocytes were sorted on the basis of CD14 on a MoFlo Astrios flow cytometer and cultured in GMP DC medium (CellGenix) with 800 U/mL GM-CSF and 400 U/mL IL-4 (CellGenix). Five days after differentiation, DCs were matured with GMC-CSF, IL-4, IL-6 (1 ng/mL), IL-1β (1 ng/mL), TNFα (1 ng/mL) and PGE1 (0.5 μg/mL). DCs were seeded at $2*10^4$ cells / well and loaded with Geltrex or 40 Gy dissociated and irradiated tumor or healthy organoid cells ($2*10^4$ cells/well). Two days later, $1*10^5$ T cells were added to each well and cultured for 24h. T cells were assayed for CD137 expression as described under flow cytometry.

Quantification and statistical analysis

Whole exome DNA sequencing data—Reads were aligned to a reference genome (GRCh38). Somatic single nucleotide variations and indels were called using Somatic Sniper (Larson et al., 2012) and SomaticIndelDetector (GATK; McKenna et al., 2010), respectively. Variants were annotated using snpEff (Cingolani et al., 2012), version 4.3. Extra-exonic and synonymous variants were removed from further analyses. Mutational load was defined as the number of non-synonymous mutations per tumor exome. The occurrence of mutations in genes recurrently mutated in hypermutated CRC was based on the top 15 most frequently recurring significantly mutated genes according to TCGA 2012.

Live imaging—During organoid killing assays, cells were co-cultured for 3 days and imaged using a charge coupled device (CCD) camera equipped with a Zeiss AxioCam MRm camera fitted to a Zeiss Axio Observer Z1 inverted microscope. Tile scans were performed every 20 to 30 minutes followed by tile stitching after recording using Zen software. Videos were generated from the stitched tiles or regions of interest after background subtraction using ImageJ software version 1.50i (Schneider et al., 2012).

Flow cytometry—Flow cytometry data was analyzed using FlowJo version 10.

Statistical analysis—Data was analyzed using GraphPad Prism version 7. Group sizes and definition of error bars is indicated in figure legends. In indicated bar graphs, background is subtracted from signal and negative values set to zero. Statistical analysis was performed using a two-tailed Student's t test. P values <0.05 were considered significant; significance values are indicated as * ($P < 0.05$), ** ($P < 0.01$) and *** ($P < 0.001$).

Data and software availability

Whole exome DNA sequencing data is available in Table S1.

Supplementary Material

Refer to Web version on PubMed Central for supplementary material.

Acknowledgements

We thank Suzanne van der Kolk, Judith Westra, Louisa Hoes and Luuk Schipper for help in patient inclusion. We acknowledge Martijn van Baalen, Anita Pfauth and Frank van Diepen for assistance in flow cytometry. We thank Marjolijn Mertz, Lenny Brocks and Bram van den Broek for help in live imaging experiments. We would like to acknowledge Dennis Peters and Ingrid Hofland from the NKI-AVL Core Facility Molecular Pathology & Biobanking (CFMPB) for supplying NKI-AVL Biobank material and lab support. DNA sequencing was performed by Marja Nieuwland, Roel Kluin and Ron Kerkhoven. We thank Marc van de Wetering and Hubrecht Organoid Technology (HUB) for advice on organoid culture. We would like to thank Merus for provision of anti-PD-1. Thanks to Marije Marsman, Steven van Houtvin, Hylke Galema, and Koen Verhoef for support in technology transfer. Stef van Lieshout, Ewart de Bruijn and Edwin Cuppen (Hartwig Medical Foundation) performed authentication of organoid lines. Thanks to Salo Ooft, Chelsea McLean, Christina Stangl, Louisa Hoes, Luuk Schipper, Maarten Ligtenberg, David Vredevoogd, Julia Boshuijzen, Wouter Scheper, Joost van den Berg, Renate Groot, Christian Blank and Daniel Peeper for input in the design of experiments.

This work was supported by the NWO gravitation program (NWO 2012-2022) (to E.V. on behalf of CancerGenomics.nl), KWF grant HUBR2014-7006 (to E.V.), the KWF Queen Wilhelmina Award (NKI 2013-6122, to T.S.) and ERC AdG SENSIT (to T.S.).

References

Alexandrov LB, Nik-Zainal S, Wedge DC, Aparicio SA, Behjati S, Biankin AV, Bignell GR, Bolli N, Borg A, Børessen-Dale AL, et al. Signatures of mutational processes in human cancer. Nature. 2013; 500:415–421. [PubMed: 23945592]

Blank CU, Haanen JB, Ribas A, Schumacher TN. CANCER IMMUNOLOGY. The "cancer immunogram". Science. 2016; 352:658–660. [PubMed: 27151852]

Borghaei H, Paz-Ares L, Horn L, Spigel DR, Steins M, Ready NE, Chow LQ, Vokes EE, Felip E, Holgado E, et al. Nivolumab versus docetaxel in advanced nonsquamous non-small cell lung cancer. N Engl J Med. 2015; 373:1627–1639. [PubMed: 26412456]

Brea EJ, Oh CY, Manchado E, Budh S, Gejman RS, Mo G, Mondello P, Han JE, Jarvis CA, Ulmert D, et al. Kinase regulation of human MHC class I molecule expression on cancer cells. Cancer Immunol Res. 2016; 4:936–947. [PubMed: 27680026]

Cingolani P, Platts A, Wang Ie L, Coon M, Nguyen T, Wang L, Land SJ, Lu X, Ruden DM. A program for annotating and predicting the effects of single nucleotide polymorphisms, SnpEff: SNPs in the genome of Drosophila melanogaster strain w1118; iso-2; iso-3. Fly (Austin). 2012; 6:80–92. [PubMed: 22728672]

Cohen CJ, Gartner JJ, Horovitz-Fried M, Shamalov K, Trebska-McGowan K, Bliskovsky VV, Parkhurst MR, Ankri C, Prickett TD, Crystal JS, et al. Isolation of neoantigen-specific T cells from tumor and peripheral lymphocytes. J Clin Invest. 2015; 125:3981–3991. [PubMed: 26389673]

Dangles-Marie V, Pocard M, Weiswald LB, Assayag F, Saulnier P, Judde JG, Janneau JL, Auger N, Validire P, et al. Establishment of human colon cancer cell lines from fresh tumors versus xenografts: comparison of success rate and cell line features. Cancer Res. 2007; 67:398–407. [PubMed: 17210723]

Dierssen JW, de Miranda NF, Ferrone S, van Puijenbroek M, Cornelisse CJ, Fleuren GJ, van Wezel T, Morreau H. HNPCC versus sporadic microsatellite-unstable colon cancers follow different routes toward loss of HLA class I expression. BMC Cancer. 2007; 7:33–43. [PubMed: 17316446]

Dijkstra KK, Voabil P, Schumacher TN, Voest EE. Genomics- and transcriptomics-based patient selection for cancer treatment with immune checkpoint inhibitors. JAMA Oncology. 2016; 2:1490–1495. [PubMed: 27491050]

Dudley ME, Wunderlich JR, Shelton TE, Even J, Rosenberg SA. Generation of tumor-infiltrating lymphocyte cultures for use in adoptive transfer therapy for melanoma patients. J Immunother. 2003; 26:332–342. [PubMed: 12843795]

Garon EB, Rizvi NA, Hui R, Leighl N, Balmanoukian AS, Eder JP, Patnaik A, Aggarwal C, Gubens M, Horn L, et al. Pembrolizumab for the treatment of non–small-cell lung cancer. N Engl J Med. 2015; 372:2018–2028. [PubMed: 25891174]

Gjorevski N, Sachs N, Manfrin A, Giger S, Bagina ME, Ordóñez-Morán P, Clevers H, Lutolf MP. Designer matrices for intestinal stem cell and organoid culture. Nature. 2016; 539:560–564. [PubMed: 27851739]

Govindan R, Ding L, Griffith M, Subrmanian J, Dees ND, Kanchi KL, Maher CA, Fulton R, Fulton L, Wallis J, et al. Genomic landscape of non-small cell lung cancer in smokers and never-smokers. Cell. 2012; 150:1121–1134. [PubMed: 22980976]

Gros A, Parkhurst MR, Tran E, Pasetto A, Robbins PF, Ilyas S, Prickett TD, Gartner JJ, Crystal JS, Roberts IM, et al. Prospective identification of neoantigen-specific lymphocytes in the peripheral blood of melanoma patients. Nat Med. 2016; 22:433–438. [PubMed: 26901407]

Patel SA, Minn AJ. Combination cancer therapy with immune checkpoint blockade: mechanisms and strategies. Immunity. 2018; 48:417–433. [PubMed: 29562193]

Horvath P, Aulner N, Bickle M, Davies AM, Nery ED, Ebner D, Montoya MC, Östling P, Pietiäinen V, Price LS, et al. Screening out irrelevant cell-based models of disease. Nature Rev Drug Discov. 2016; 15:751–769. [PubMed: 27616293]

Larkin J, Chiarion-Sileni V, Gonzalez R, Grob JJ, Cowey CL, Lao CD, Schadendorf D, Dummer R, Smylie M, Rutkowski P, et al. Combined nivolumab and ipilimumab or monotherapy in untreated melanoma. N Engl J Med. 2015; 373:23–34. [PubMed: 26027431]

Larson DE, Harris CC, Chen K, Koboldt DC, Abbott TE, Dooling DJ, Ley TJ, Mardir ER, Wilson RK, Ding L. SomaticSniper: identification of somatic point mutations in whole genome sequencing data. Bioinformatics. 2012; 28:311–317. [PubMed: 22155872]

Le DT, Durham JN, Smith KN, Wang H, Bartlett BR, Aulakh LK, Lu S, Kemberling H, Wilt C, Luber BS, et al. Mismatch repair deficiency predicts response of solid tumors to PD-1 blockade. Science. 2017; 357:409–413. [PubMed: 28596308]

Le DT, Uram JN, Wang H, Bartlett BR, Kemberling H, Eyring AD, Skora AD, Luber BS, Azad NS, Laheru D, et al. PD-1 blockade in tumors with mismatch-repair deficiency. N Engl J Med. 2015; 28:11–13.

Liang-Chu MMY, Yu M, Haverty PM, Koeman J, Ziegle J, Lee M, Bourgon R, Neve RM. Human biosample authentication using the high-throughput, cost-effective SNPTrace™ system. PLoS One. 2015; 10:e0116218. [PubMed: 25714623]

McKenna A, Hanna M, Banks E, Sivachenko A, Cibulskis K, Kernytsky A, Garimella K, Altshuler D, Gabriel S, Daly M, et al. The Genome Analysis Toolkit: a MapReduce framework for analyzing next-generation DNA sequencing data. Genome Res. 2010; 20:1297–1303. [PubMed: 20644199]

Ogino S, Noshiko K, Irahara N, Meyerhardt JA, Baba Y, Shima K, Glickman JN, Ferrone CR, Mino-Kenudson M, Tanaka N, et al. Lymphocytic reaction to colorectal cancer is associated with longer survival, independent of lymph node count, microsatellite instability, and CpG island methylator phenotype. Clin Cancer Res. 2009; 15:6412–6420. [PubMed: 19825961]

Overman MJ, McDermott R, Leach JL, Lonardi S, Lenz HJ, Morse MA, Desai J, Hill A, Axelson M, Moss RA, et al. Nivolumab in patients with metastatic DNA mismatch repair-deficient or microsatellite instability-high colorectal cancer (Check Mate 142): an open-label, multicentre, phase 2 study. Lancet Oncol. 2017; 18:1182–1191. [PubMed: 28734759]

Overman MJ, Lonardi S, Wong KYM, Lenz HJ, Gelsomino F, Aglietta M, Morse MA, van Cutsem E, McDermott R, Hill A, et al. Durable clinical benefit with nivolumab plus ipilimumab in DNA mismatch repair-deficient/microsatellite instability-high metastatic colorectal cancer. J Clin Oncol. 2018; 36:773–779. [PubMed: 29355075]

Pitt J, Vétizou M, Daillére R, Roberti MP, Yamazaki T, Routy B, Lepage P, Boneca IG, Chamaillard M, Kroemer G, et al. Resistance mechanisms to immune checkpoint blockade in cancer: tumor-intrinsic and –extrinsic factors. Immunity. 2016; 44:1255–1269. [PubMed: 27332730]

Ritter C, Fan K, Paschen A, Reker Hardrup S, Ferrone S, Nghiem P, Ugurel S, Schrama D, Becker JC. Epigenetic priming restores the HLA class-I antigen presenting machinery expression in Merkel cell carcinoma. Sci Reports. 2017; 7:2290–2300.

Rosenberg SA, Restifo NP. Adoptive cell transfer as personalized immunotherapy for human cancer. Science. 2015; 348:62–68. [PubMed: 25838374]

Sachs N, Zomer-van Ommen DD, Papaspyropoulos A, Heo I, Bottinger L, Klay D, Weeber F, Huelsz-Prince G, Lakobachvili N, Viveen MC, et al. Long-term expanding human airway organoids for disease modeling. bioRxiv. 2018 May 9.doi: 10.1101/318444

Schumacher TN, Schreiber RD. Neoantigens in cancer immunotherapy. Science. 2015; 348:69–74. [PubMed: 25838375]

Schneider CA, Rasband WS, Eliceiri KIW. NIH Image to ImageJ: 25 years of image analysis. Nature Methods. 2012; 9:671–675. [PubMed: 22930834]

Sharma P, Allison JP. Immune checkpoint targeting in cancer therapy. Cell. 2015; 161:205–214. [PubMed: 25860605]

Sharma P, Hu-Lieskovan S, Wargo J, Ribas A. Primary, adaptive, and acquired resistance to cancer immunotherapy. Cell. 2017; 168:707–723. [PubMed: 28187290]

Stevanovic S, Draper LM, Langhan MM, Campbell TE, Kwong ML, Wunderlich JR, Dudley ME, Yang JC, Sherry RM, Kammula US, et al. Complete regression of metastatic cervical cancer after treatment with human papillomavirus-targeted tumor-infiltrating T cells. J Clin Oncol. 2015; 10:1543–1550.

Szolek A, Schubert B, Mohr C, Sturm M, Feldhahn M, Kohlbacher O. Bioinformatics. 2014; 1:3310–3316.

Tanabe H, Takada Y, Minegishi D, Kurematsu M, Masui T, Mizusawa H. Cell line individualization by STR multiplex system in the cell bank found cross-contamination between ECV304 and EJ-1/T24. Tiss Cult Res Commun. 1999; 18:329–338.

The Cancer Genome Atlas Network. Comprehensive molecular characterization of human colon and rectal cancer. Nature. 2012; 487:330–337. [PubMed: 22810696]

Verdegaal EM, Visser M, Ramwadhdoebé TH, van der Minne CE, van Steijn JA, Kapiteijn E, Haanen JB, van der Burg SH, Nortier JW, Osanto S. Successful treatment of metastatic melanoma by adoptive transfer of blood-derived polyclonal tumor-specific $CD4^+$ and $CD8^+$ T cells in combination with low-dose interferon-alpha. Cancer Immunol Immunother. 2011; 60:953–963. [PubMed: 21431917]

Vogelstein B, Papadopoulos N, Velculescu VE, Zhou S, Diaz LA Jr, Kinzler KW. Cancer genome landscapes. Science. 2013; 339:1546–1558. [PubMed: 23539594]

Weeber F, van de Wetering M, Hoogstraat M, Dijkstra KK, Krijgsman O, Kuilman T, Gadellaa-van Hooijdonk CG, van der Velden DL, Peeper DS, Cuppen EP, et al. Preserved genetic diversity in organoids cultured from biopsies of human colorectal cancer metastases. Proc Natl Acad U S A. 2015; 112:13308–13311.

Van de Wetering M, Francies HE, Francis JM, Bounova G, Iorio F, Pronk A, van Houdt W, van Gorp J, Taylor-Weiner A, Kester L, et al. Prospective derivation of a living biobank of colorectal cancer patients. Cell. 2015; 161:933–945. [PubMed: 25957691]

Zaretsky JM, Garcia-Diaz A, Shin DS, Escuin-Ordinas H, Hugo W, Hu-Lieskovan S, Torrejon DY, Abril-Rodriguez G, Sandoval S, Barthly L, et al. Mutations associated with acquired resistance to PD-1 blockade in melanoma. N Engl J Med. 2016; 375:819–829. [PubMed: 27433843]

Zheng C, Sun YH, Ye XL, Chen HQ, Ji HB. Establishment and characterization of primary lung cancer cell lines from Chinese population. Acta Pharmacologica Sinica. 2011; 32:385–392. [PubMed: 21372829]

Europe PMC Funders Author Manuscripts

Europe PMC Funders Author Manuscripts

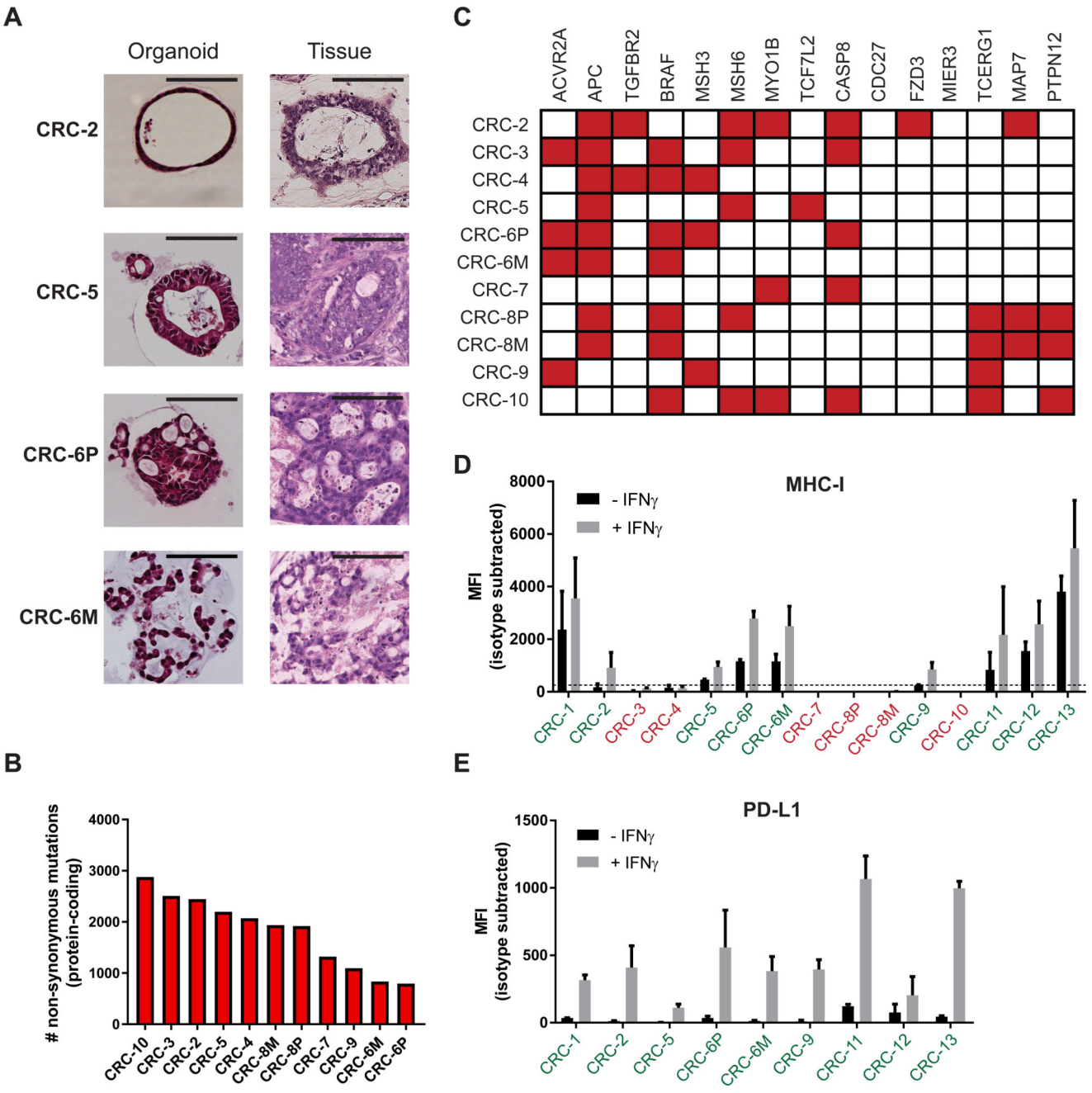

Figure 1. Characterization of a panel of dMMR CRC organoids.

(A) Haematoxylin and eosin (H&E) staining of tumor organoids and original tumor tissue. Organoids show morphology similar to the architecture of the original tumor. CRC-2 organoids demonstrates cystic tubules similar to mucin-filled glands of the primary tumor. CRC-5 organoids and primary tumor are composed of tubular glands with layered epithelium. Organoid CRC-6P is composed of complex cribriform glands, also seen in the primary tumor. Organoid CRC-6M consists of irregular trabecular structures and poorly formed glands, similar to the metastasis. Scale bar = 100 μm.

Europe PMC Funders Author Manuscripts

(B) Mutational load of tumor organoids as determined by the number of non-synonymous mutations per tumor exome.
(C) Mutation status of genes significantly mutated in hypermutated colorectal cancer according to TCGA 2012. Mutated genes are indicated in red.
(D) Cell surface MHC-I expression as determined by flow cytometry. Organoids were stimulated with 200 ng/mL IFNγ for 24 hours or left unstimulated. Bar graphs indicate median fluorescence intensity (MFI) of anti-HLA-A,B,C-PE minus MFI of isotype control. Tumor organoids with MFI < 250 above isotype control (dashed line) were classified as MHC-I deficient (indicated in red). Error bars indicate s.e.m. of at least two independent experiments.
(E) Cell surface PD-L1 expression as determined by flow cytometry. Organoids were stimulated with 200 ng/mL IFNγ for 24 hours or left unstimulated. Bar graphs indicate median fluorescence intensity (MFI) of anti-PD-L1-APC minus MFI of isotype control. Error bars indicate s.e.m. of at least two independent experiments.
See also Figures S1-S2 and Tables S1-S2.

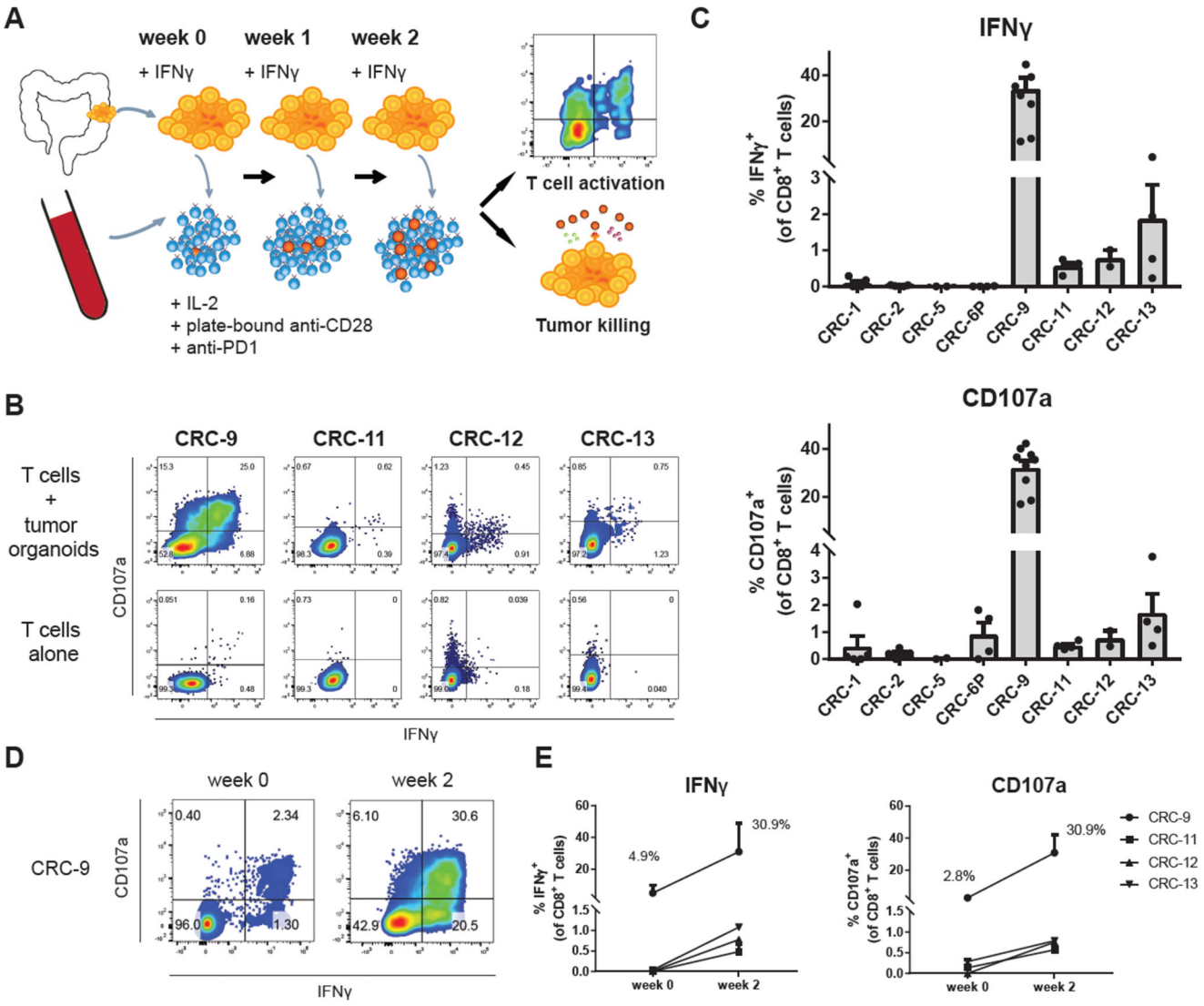

Figure 2. Induction of tumor reactivity in circulating T cells by co-culture with autologous tumor organoids.

(A) Experimental workflow. Tumor organoids were established from dMMR CRC (resections or biopsies of primary tumors or metastases) and stimulated with IFNγ for 24 hours prior to co-culture with peripheral blood lymphocytes (PBL) from the same patient. PBL were stimulated weekly with fresh tumor cells. After two weeks of co-culture, T cell effector functions and sensitivity of tumor organoids to T cell-mediated killing were evaluated using flow cytometry.

(B) Representative flow cytometry plots gated on $CD8^+$ T cells tested for reactivity against autologous organoids after two weeks of co-culture with autologous tumor organoids.

(C) Quantification of organoid-induced IFNγ production and CD107a cell surface expression of $CD8^+$ T cells obtained by two week co-culture with autologous tumor organoids. Background (spontaneous IFNγ production or CD107a expression) is subtracted

Europe PMC Funders Author Manuscripts

from signal. Error bars indicate s.e.m. of at least 2 biological replicates. Dots indicate biological replicates.

(D) Flow cytometry plots gated on $CD8^+$ T cells of patient CRC-9 tested for reactivity against autologous organoids directly after PBL isolation, or after two weeks of co-culture with autologous tumor organoids.

(E) Quantification of organoid-induced IFNγ production and CD107a cell surface expression of $CD8^+$ T cells directly after PBL isolation, or obtained by two week co-culture with autologous tumor organoids. Background (spontaneous IFNγ production or CD107a expression) is subtracted from signal. Error bars indicate s.e.m of n = 2 biological replicates for CRC-9 and CRC-11. N = 1 for CRC-12 and CRC-13 (low amount of blood available).

Europe PMC Funders Author Manuscripts

Europe PMC Funders Author Manuscripts

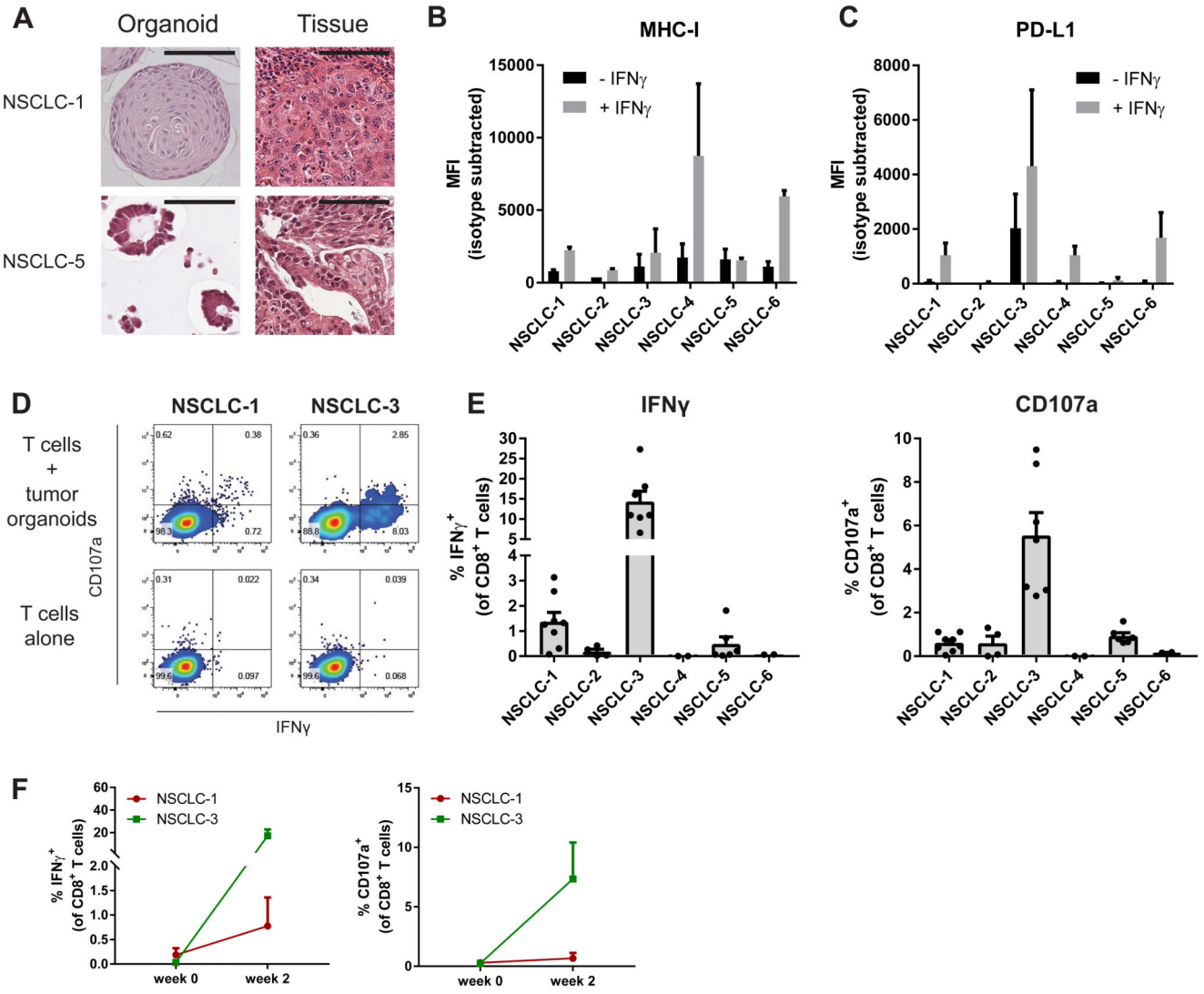

Figure 3. Induction of tumor reactivity in circulating T cells from patients with NSCLC.

(A) Haematoxylin and eosin staining of tumor organoids and original tumor tissue. Organoids show morphology similar to the architecture of the original tumor. NSCLC-1 organoids consists of large cells forming a solid mass, similar to the primary tumor. NSCLC-5 organoids are composed of tubular glands similar to the original tumor. Scale bar = 100 μm.

(B-C) Cell surface MHC-I (B) and PD-L1 (C) expression as determined by flow cytometry. Organoids were stimulated with 200 ng/mL IFNγ for 24 hours or left unstimulated. Bar graphs indicate median fluorescence intensity (MFI) of anti-HLA-A,B,C-PE or anti-PD-L1-APC minus MFI of isotype control. Error bars indicate s.e.m. of two independent experiments.

(D) Representative flow cytometry plots gated on $CD8^+$ T cells tested for reactivity against autologous organoids after two weeks of co-culture with autologous tumor organoids.

(E) Quantification of organoid-induced IFNγ production and CD107a cell surface expression of $CD8^+$ T cells obtained by two week co-culture with autologous tumor

organoids. Background (spontaneous IFNγ production or CD107a expression) is subtracted from signal. Error bars indicate s.e.m. of at least 2 biological replicates. Dots indicate biological replicates.

(F) Quantification of organoid-induced IFNγ production and CD107a cell surface expression of $CD8^+$ T cells directly after PBL isolation, or obtained by two week co-culture with autologous tumor organoids. Background (spontaneous IFNγ production or CD107a expression) is subtracted from signal. Error bars indicate s.e.m of n = 2 biological replicates. See also Figure S3.

Europe PMC Funders Author Manuscripts

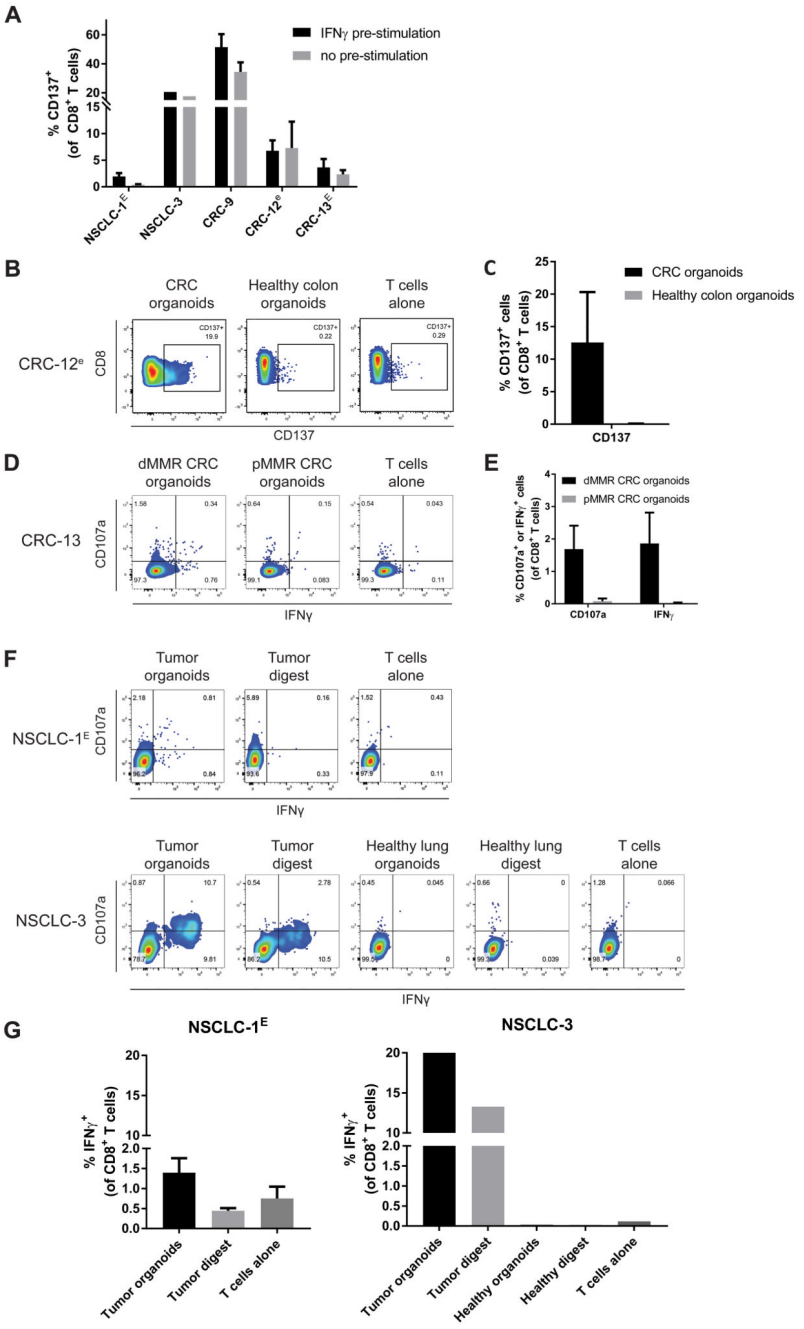

Figure 4. Specificity of organoid-reactive T cell responses.

T cells were obtained by two week co-culture with autologous tumor organoids. To increase the number of T cells available for testing, where indicated (lower case e) tumor-reactive T cells were then expanded using a rapid expansion protocol (Dudley et al. 2013), in some cases preceded by CD137-based enrichment of tumor-reactive cells (indicated by upper case E).

(A) T cells were challenged with organoids pre-stimulated with 200 ng/mL IFNγ for 24 hours or with unstimulated organoids and evaluated for expression of the activation marker

CD137. Background (percentage positive cells in T cells alone control) is subtracted from signal. Error bars indicate s.e.m. of at least 2 biological replicates.

(B) Representative flow cytometry plots of $CD8^+$ T cells stimulated with either tumor organoids or healthy colon organoids.

(C) Quantification of CD137 expression by $CD8^+$ T cells stimulated with either tumor organoids or healthy colon organoids. Background (percentage positive cells in T cells alone control) is subtracted from signal. Error bars indicate s.e.m. of 2 biological replicates. One of the replicates for T cells stimulated with tumor organoids is the same as data in (A).

(D) Representative flow cytometry plots of $CD8^+$ T cells obtained by two weeks of co-culture with mismatch repair deficient (dMMR) CRC organoids that were re-stimulated with either dMMR CRC organoids or mismatch repair proficient (pMMR) CRC organoids.

(E) Quantification of organoid-induced IFNγ production and CD107a cell surface expression of $CD8^+$ T cells obtained by two weeks of co-culture with mismatch repair deficient (dMMR) CRC organoids that were re-stimulated with either dMMR CRC organoids or mismatch repair proficient (pMMR) CRC organoids. Background (percentage positive cells in T cells alone control) is subtracted from signal. Error bars indicate s.e.m. of 4 biological replicates. Data for T cells stimulated with dMMR CRC organoids is the same as data in Figure 2A.

(F) Representative flow cytometry plots of $CD8^+$ T cells stimulated with either tumor digest, normal lung digest, NSCLC organoids or healthy lung organoids.

(G) Quantification of IFNγ production of $CD8^+$ T cells stimulated with either tumor digest, normal lung digest, NSCLC organoids or healthy lung organoids. Error bars represent s.d. of technical replicates.

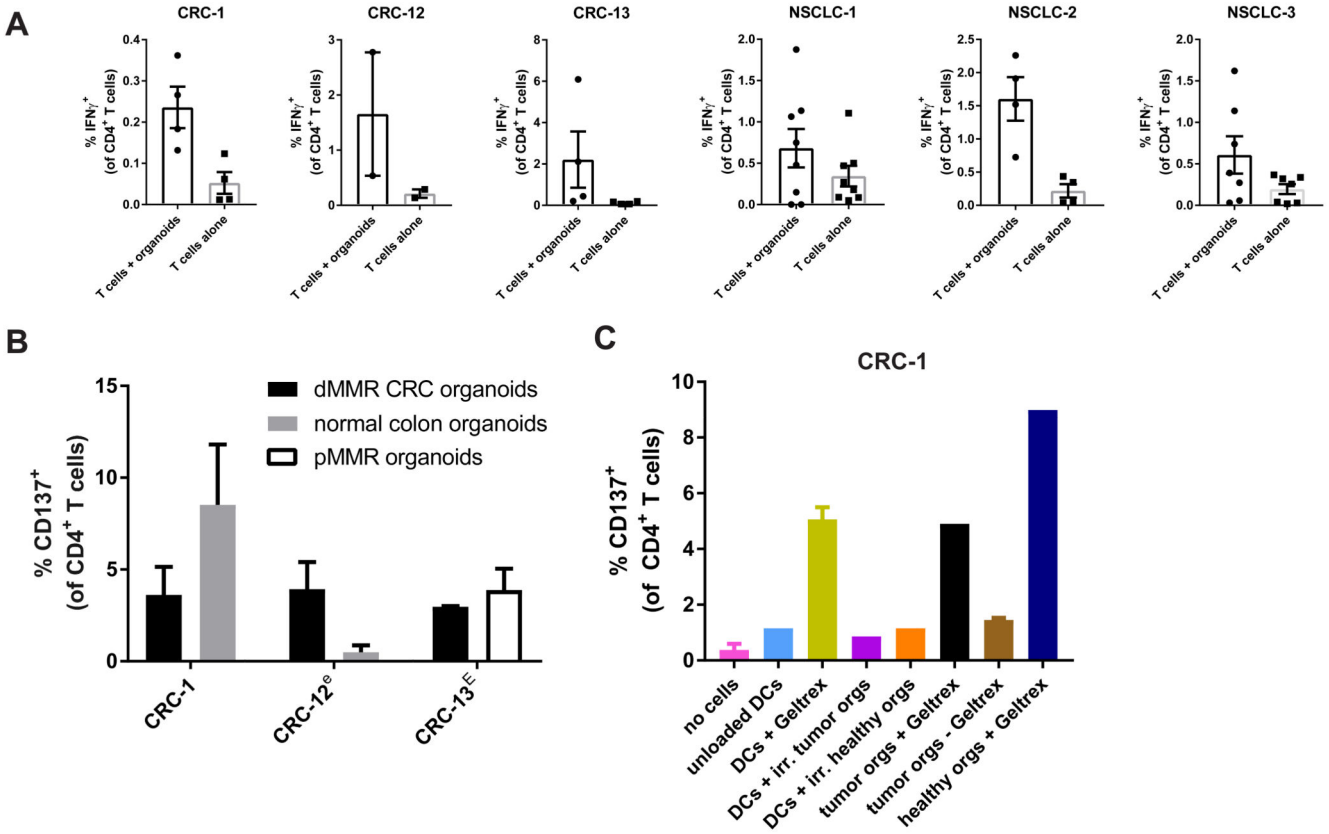

Figure 5. CD4$^+$ T cell reactivity against xenogeneic tissue culture components.

(A) Quantification of spontaneous and organoid-induced IFNγ production by CD4$^+$ T cells obtained by two week co-culture with autologous tumor organoids. Error bars indicate s.e.m. of at least 2 biological replicates.

(B) Quantification of CD137 expression by CD4$^+$ T cells upon re-stimulation with the tumor organoids used for induction, normal colon organoids, or organoids of a mismatch repair proficient (pMMR) CRC from the same patient. T cells were obtained by two week co-culture with autologous tumor organoids and where indicated (lower case e) further expanded using a rapid expansion protocol (Dudley et al. 2013), in some cases preceded by CD137-based enrichment of tumor-reactive cells (indicated by upper case E). Error bars indicate s.e.m. of at least 2 biological replicates.

(C) Quantification of CD137 expression by CD4$^+$ T cells after stimulation with unloaded or Geltrex-loaded monocyte-derived dendritic cells (DCs), irradiated tumor cells, or organoids cultured with or without Geltrex. Error bars indicate s.d. of technical replicates.

See also Figure S4.

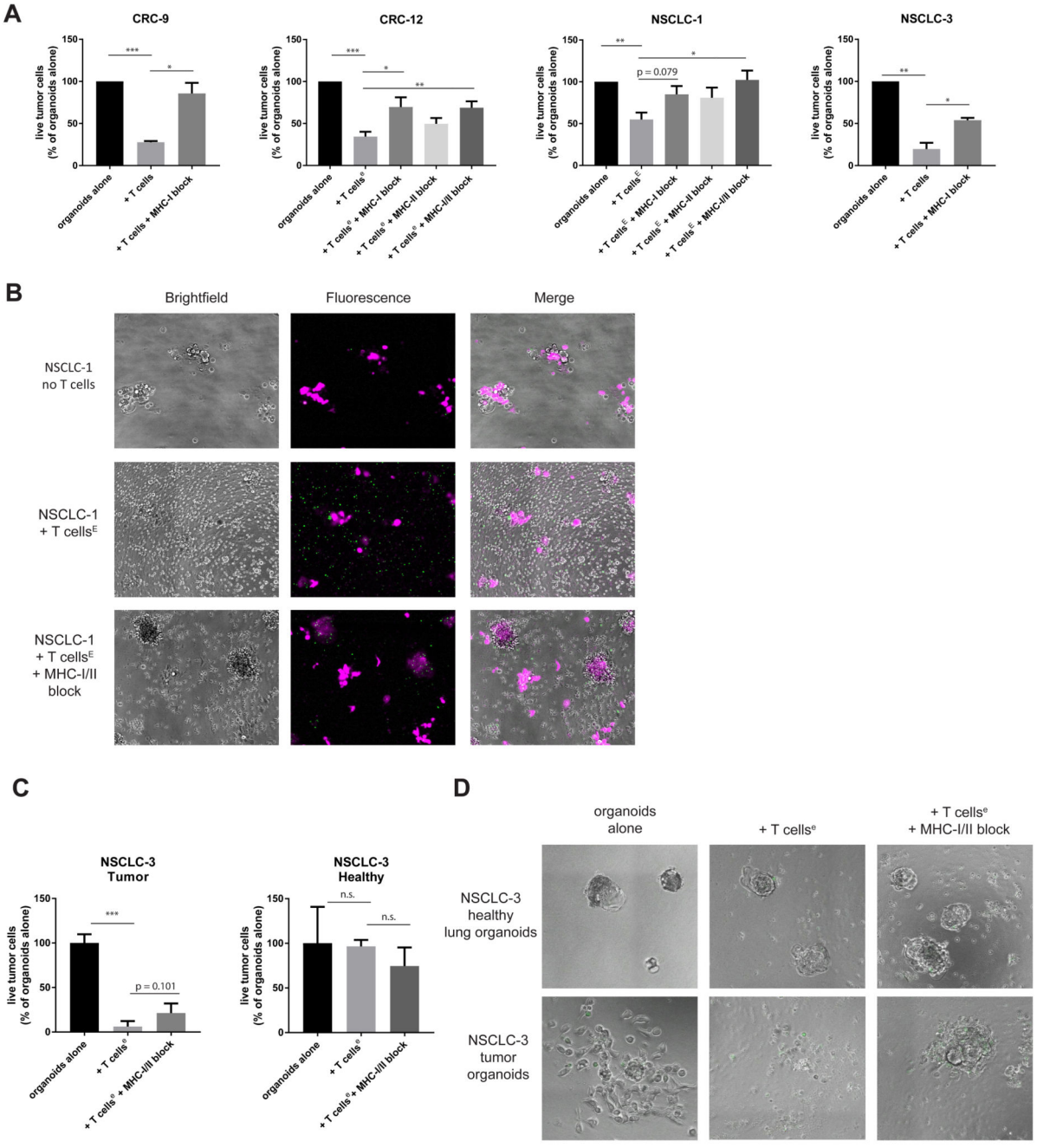

Figure 6. Tumor organoids are killed by autologous tumor-reactive T cells.

T cells were obtained by two week co-culture with autologous tumor organoids and where indicated (lower case e) further expanded using a rapid expansion protocol (Dudley et al. 2013), in some cases preceded by CD137-based enrichment of tumor-reactive cells (indicated by upper case E).

(A) Quantification of organoid killing upon T cell co-culture. After 3 days of co-culture, organoids were dissociated into single cells and the number of live cells was quantified using flow cytometry in the presence of counting beads. Where indicated, MHC-I or MHC-II was

Europe PMC Funders Author Manuscripts

blocked with W6/32 or Tü39 antibody, respectively. * $p < 0.05$, ** $p < 0.01$, *** $p < 0.001$, Student's t test. Error bars indicate s.e.m. of at least two biological replicates.
(B) Microphotographs of NSCLC-1 organoids 72 hours after culture with or without T cells in the presence of a green-fluorescent caspase 3/7 probe. Organoids were labelled with CellTrace Yellow (magenta) prior to co-culture. Note the appearance of apoptotic (green) cells upon addition of T cells. When MHC-I and MHC-II are blocked, T cells cluster around organoids but apoptosis is reduced and organoids remain larger in size.
(C) Quantification of killing of matched NSCLC and healthy lung organoids as in (A). Representative of two independent experiments. Error bars indicate s.d. of technical replicates.
(D) Microphotograph images of NSCLC-3 healthy and tumor organoids 72 hours after culture with or without T cells in the presence of a green-fluorescent caspase 3/7 probe. See also Figure S5.

Europe PMC Funders Author Manuscripts

Europe PMC Funders Author Manuscripts

Table 1

Characteristics of panel of dMMR CRC samples.

MLH1: mutL homolog 1; PMS2: PMS1 homolog 2, mismatch repair system component; MSH2: mutS homolog 2; MSH6: mutS homolog 6. F: female; M: male.

Sample	Sex	Age	Tumor location	Stage	Primary tumor / metastasis	Biopsy / resection	Absent MMR stains
CRC-1	F	68	Colon	I	Primary tumor	Resection	MLH1/PMS2
CRC-2	M	65	Colon	III	Primary tumor	Resection	MSH6
CRC-3	F	65	Colon	II	Primary tumor	Resection	MLH1/PMS2
CRC-4	F	75	Colon	III	Primary tumor	Resection	MLH1/PMS2
CRC-5	F	73	Rectum	I	Primary tumor	Resection	MSH6
CRC-6P	F	67	Colon	IV	Primary tumor	Resection	MLH1/PMS2
CRC-6M	F	67	Peritoneum	IV	Metastasis	Resection	MLH1/PMS2
CRC-7	F	62	Colon	III	Primary tumor	Resection	MLH1/PMS2
CRC-8P	M	50	Colon	IV	Primary tumor	Resection	MLH1/PMS2
CRC-8M	M	50	Liver	IV	Metastasis	Resection	MLH1/PMS2
CRC-9	F	51	Lymph node (neck)	IV	Metastasis	Biopsy	MLH1/PMS2
CRC-10	F	66	Liver	IV	Metastasis	Biopsy	MLH1/PMS2 (partial loss of MSH6)
CRC-11	F	66	Peritoneum	IV	Metastasis	Biopsy	MLH1/PMS2
CRC-12	F	74	Colon	I	Primary tumor	Resection	MLH1/PMS2
CRC-13	F	70	Colon	II	Primary tumor	Biopsy	MLH1/PMS2